ChemComm

FEATURE ARTICLE

Check for updates

Insights into type I photoreactivity of cyclometalated iridium(III) and ruthenium(II) photosensitizers

Gloria Vigueras, [ID] *[a] Vicente Marchán [ID] [bc] and José Ruiz [ID] *[a]

Photodynamic therapy (PDT) is a light-activated treatment that relies on the generation of cytotoxic reactive oxygen species (ROS). While most clinically approved photosensitizers (PSs) operate through a type II mechanism—based on energy transfer to molecular oxygen—their efficacy is often compromised in hypoxic tumor microenvironments. In this context, type I PSs capable of initiating electron or hydrogen atom transfer reactions have gained increasing attention due to their reduced dependency on oxygen levels. In this Feature Article, we review recent advances in cyclometalated iridium- and ruthenium-based PSs exhibiting type I photoreactivity, highlighting representative examples from both our own work and the literature. Although rational design strategies are still emerging, selected examples demonstrate how subtle modifications in complex architecture, ligand environment, or metal center identity can influence the balance between type I and type II pathways. In particular, we outline conceptual design motifs—such as cyclometalation with thiophenyl-based ligands, conjugation with fluorophores such as coumarin or BODIPY, and multinuclear architectures—that have been explored to enhance electron-transfer reactivity under hypoxic conditions. Beyond photophysical considerations, we discuss common challenges in the experimental identification of type I mechanisms and emphasize the importance of biologically relevant models, such as 3D cell cultures, for evaluating PS performance. Ultimately, we offer a perspective on how molecular design can be tailored to meet the demands of next-generation PDT agents, aiming to improve therapeutic outcomes in low-oxygen tumor microenvironments, which are characteristic of highly aggressive and treatment-resistant tumors.

[a] Departamento de Química Inorgánica, Universidad de Murcia, Biomedical Research Institute of Murcia (IMIB-Arrixaca), E-30100 Murcia, Spain.
E-mail: gloria.vigueras@um.es, jruiz@um.es

[b] Departament de Química Inorgànica i Orgànica, Secció de Química Orgànica, Universitat de Barcelona (UB), Institut de Biomedicina de la Universitat de Barcelona (IBUB), Martí i Franquès 1-11, E-08028 Barcelona, Spain

[c] Serra Húnter Professor, Universitat de Barcelona, E-08028 Barcelona, Spain

Gloria Vigueras

Gloria Vigueras Bautista received her PhD with distinction in chemistry from the University of Murcia in 2021, where she developed phosphorescent iridium(III) complexes for therapy and photodynamic therapy of cancer. Her recent research as Marie Skłodowska-Curie Postdoctoral Fellow (2023–2025) in ChimieParisTech (France), established novel approaches in antimicrobial photodynamic inactivation with applications in agricultural biotechnology. Her multidisciplinary expertise spans from anticancer metallodrugs to advanced photoinactivation strategies against resistant microorganisms.

Vicente Marchán

Vicente Marchán received his BSc and PhD in Chemistry from the University of Barcelona (UB), both awarded with the Extraordinary Prize. Following a postdoctoral stay at the US Food and Drug Administration, he joined UB as Associate Professor and is currently Full Professor and member of its Institute of Biomedicine. His research focuses on the development of light-activatable chemical tools for bioimaging and therapeutic applications, with a particular focus on photodynamic therapy and photopharmacology using organic fluorophores and metal complexes. He has authored over 70 publications in high-impact journals and is co-inventor of three patents.

1. Introduction

Tumor hypoxia represents a major barrier to effective cancer treatment.[1] It refers to regions within solid tumors characterized by low oxygen levels, resulting from the rapid proliferation of cancer cells and inadequate vascularization.[2] While oxygen concentration in normal tissues typically ranges from 2–9% (40 mmHg pO_2), levels in the tumor microenvironment can drop to as low as 0.02–2% O_2 (below 2.5 mmHg pO_2).[3] This oxygen deficiency triggers adaptive responses that promote tumor survival, angiogenesis, metastasis, and resistance to conventional anticancer therapies, ultimately contributing to poor patient prognosis.

Photodynamic therapy (PDT) is a minimally invasive therapeutic modality that has emerged as a promising strategy for cancer treatment. PDT relies on the interplay of three essential components: a photosensitizer (PS), a light source, and molecular oxygen. Although most clinical PDT approaches have traditionally focused on oxygen-dependent mechanisms, recent research highlights the growing importance of oxygen-independent pathways as critical alternatives for overcoming challenges posed by hypoxic tumor microenvironments.[4]

At the core of PDT are two principal photochemical pathways: type II, which involves energy transfer from the PS's excited triplet state to molecular oxygen to generate singlet oxygen, and type I, characterized by electron or hydrogen transfer leading to reactive radical species (Fig. 1). Yet, beneath the apparent simplicity of this dichotomy lies a complex interplay of photophysical, photochemical and biochemical processes, often governed by the presence and availability of molecular oxygen.[5,6] A crucial step common to both mechanisms is the efficient population of the PS's triplet excited state, which depends on effective intersystem crossing (ISC) from the singlet state. Enhancing ISC is therefore fundamental to improving reactive oxygen species (ROS) generation. One widely adopted strategy involves increasing spin–orbit coupling (SOC), which facilitates ISC; this can be efficiently achieved by incorporating heavy atoms—particularly transition metals—into the PS structure.[7] These metal centers promote SOC due to their high atomic number, making them especially attractive for designing triplet-active compounds. Alternatively, reinforcing the intramolecular charge-transfer (ICT) character of the PS can also boost ISC efficiency by narrowing the singlet–triplet energy gap (ΔE_{S-T}).[8,9] This is typically accomplished through the strategic placement of electron-donating or electron-withdrawing groups within the PS structure, although transition metals themselves can also modulate ICT behavior *via* metal–ligand interactions. Thus, metal-based PSs offer a multifaceted approach to engineering efficient triplet-state PSs.[10]

In 2018, Li *et al.* proposed type I PDT as a "partial oxygen-recyclable" mechanism mediated by superoxide radicals (Fig. 2), offering a compelling explanation for how type I photoprocesses can help overcome PDT resistance under hypoxic conditions.[11,12] This renewed interest in type I PDT has stimulated efforts to design PSs capable of engaging in both type I and type II pathways, thereby enabling the generation of a broader spectrum of ROS beyond singlet oxygen—including superoxide ($^{\bullet}O_2^-$) and hydroxyl ($^{\bullet}OH$) radicals—that remain effective even in oxygen-deficient tumor microenvironments.

This growing interest in type I PDT has underscored the value of systems that can efficiently participate in electron transfer reactions. In this context, transition metal complexes stand out not only for their ability to access long-lived triplet excited states, but also for their intrinsic electronic configurations—particularly the presence of partially filled d orbitals—which facilitate interactions with nearby biomolecules and molecular oxygen species.[12] These features make them uniquely well-suited to mediate type I processes, especially under hypoxic conditions, where classical $^1O_2$ production becomes inefficient.

Nevertheless, the development of type I PSs faces several challenges due to inconsistent interpretations of mechanisms, varied detection techniques, and diverse application strategies. This evolving understanding compels us to reconsider the design principles of metal-based PSs, scrutinizing how their electronic structures and ligand environments influence photoreactivity toward electron-transfer pathways.

Several comprehensive reviews on noble-metal complexes for PDT have been published recently.[13,14] In contrast, this Feature Article adopts a more focused and intentional scope: it explores cyclometalated Ir(III) and Ru(II) complexes that exhibit type I photoreactivity. Particular attention is given to mechanistic insights, representative examples (including our own contributions), and the experimental challenges involved in identifying type I behavior under biologically relevant conditions. While our primary focus is on cyclometalated Ir(III) and Ru(II) complexes, recent advances in other metal-based platforms also deserve brief mention. Platinum(II)[15] and osmium(II)[16] PSs have been investigated for oxygen-independent photoreactivity within specific ligand environments, while cobalt(III)-based systems, as well as certain manganese(II) and iron(III) compounds are gaining interest due to their natural abundance and cost effectiveness.[17–20] These examples illustrate that type I photoreactivity is not exclusive to Ir

José Ruiz, Full Professor at UMU, earned his Chemistry degree with honours and was awarded the National Extraordinary Prize. He founded the Metallodrugs Discovery Group and leads pioneering research at IMIB. His development of iridium(II) and ruthenium(II) complexes has advanced cancer therapy and photodynamic treatment, culminating in 140 publications (h-index 43, over 5100 citations) in high-impact journals. He collaborates internationally, evaluates for leading journals and funding agencies, and mentors PhD students now thriving in global positions. As Chair of the RSEQ Murcia section, he actively promotes science outreach through regional Chemistry Olympiads and educational initiatives.
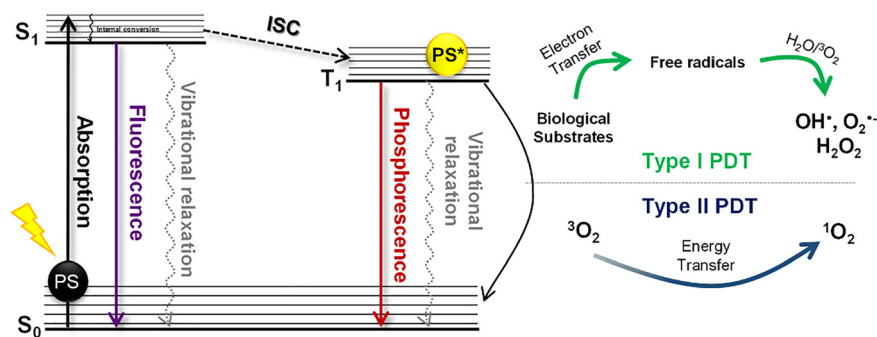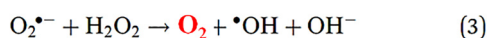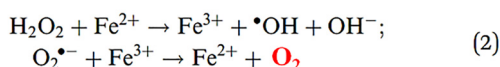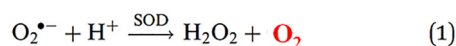
José Ruiz

Fig. 1 Jablonski diagram illustrating type I and type II photochemical pathways of PDT. Adapted from ref. 46 with permission from the Royal Society of Chemistry, copyright 2025.

Type I PDT:
a "partial oxygen-recyclable mechanism"

$$O_2^{\bullet-} + H^+ \xrightarrow{SOD} H_2O_2 + O_2 \quad\quad (1)$$

$$H_2O_2 + Fe^{2+} \rightarrow Fe^{3+} + {}^{\bullet}OH + OH^-;$$
$$O_2^{\bullet-} + Fe^{3+} \rightarrow Fe^{2+} + O_2 \quad\quad (2)$$

$$O_2^{\bullet-} + H_2O_2 \rightarrow O_2 + {}^{\bullet}OH + OH^- \quad\quad (3)$$

(1) Disproportionation reaction
(2) Fenton reactions
(3) H_2O_2 reduction through the Haber–Weiss reaction

Fig. 2 Type I "partial oxygen-recyclable" mechanism proposed by Li et al.[11,12] ${}^{\bullet}O_2^-$ generated during type I photoreactions can undergo disproportionation catalyzed by superoxide dismutase (SOD), producing both H_2O_2 and molecular oxygen. Additionally, ${}^{\bullet}O_2^-$ may react with H_2O_2 via Fenton- or Haber–Weiss-type chemistry, leading to the formation of ${}^{\bullet}OH$.

and Ru complexes. They also help contextualize the unique opportunities and challenges associated with cyclometalated platforms.

2. What defines a type I photosensitizer? Molecular features and design strategies

Type I PSs are characterized by their ability to generate ROS predominantly through electron or hydrogen transfer mechanisms, rather than via direct energy transfer to molecular oxygen (Fig. 1). In the canonical type I pathway, the excited triplet state ($^3PS^*$) transfers electrons to surrounding oxygen or water molecules, producing superoxide ($^{\bullet}O_2^-$), hydroxyl ($^{\bullet}OH$) radicals and/or hydrogen peroxide (H_2O_2). These free ROS initiate oxidative cascades that can trigger lipid peroxidation, leading to the formation of peroxyl radicals ($ROO^{\bullet}$), alkoxyl radicals ($RO^{\bullet}$), etc., ultimately resulting in cell death.[21]

An alternative—but increasingly recognized—type I mechanism involves initial electron donation from endogenous biomolecules, such as NAD(P)H, amino acids, peptides, or nucleic acids, to the excited PS.[9] The resulting reduced PS intermediate subsequently transfers an electron to O_2, generating superoxide indirectly. This two-step pathway, conceptually analogous to photocatalytic redox cycles, expands the mechanistic landscape of type I PDT and underscores its adaptability in complex biological environments.

Type I and type II mechanisms often coexist within a given PS, with the relative contribution of each pathway determined by molecular structure, medium composition, and environmental conditions. In the design of organic PSs, two principal strategies have been employed to favor type I reactivity. The indirect strategy involves suppressing excited energy transfer (EET) by lowering the energy of the triplet excited state (T_1) below the threshold required to generate singlet oxygen ($^1O_2$), thereby disfavoring the type II pathway. Conversely, the direct strategy focuses on enhancing electron transfer (ET) by structurally optimizing the PS to promote efficient ET processes and the subsequent formation of type I ROS such as $^{\bullet}O_2^-$ and $^{\bullet}OH$. Several recent reviews have comprehensively explored these molecular design strategies, shedding light on the structural and electronic factors that govern type I versus type II behavior in organic PSs.[5,9,12,22,23]

Compared to the type I mechanism, the type II process is generally more kinetically favorable. This is reflected in the significantly higher rate constants for photoinduced energy transfer to molecular oxygen than for electron or hydrogen atom transfer between PSs and biological substrates. For instance, the rate constant for energy transfer (K_{EET}) from phthalocyanines to oxygen is approximately 10^9 M^{-1} s^{-1}, whereas their electron transfer rates (K_{ET}) with biological substrates typically range from 10^4 to 10^8 M^{-1} s^{-1}.[5] However, transition metal complexes can shift this mechanistic balance toward type I reactivity due to several intrinsic features: partially filled d orbitals, favorable redox potentials, and strong SOC. These properties facilitate efficient ISC and promote electron transfer processes.[21] As a result, metal-based PSs can achieve high ROS yields even under low oxygen conditions and access alternative photoreactivity pathways that are not available to purely organic systems.

Given the ongoing debate regarding the accurate identification of type I pathways, it is crucial to critically evaluate both

the reliability and the limitations of the experimental techniques commonly employed for ROS detection. These considerations are discussed in detail in Section 4.

3. Metal-based type I photosensitizers: representative examples and insights

Transition metal complexes have attracted increasing attention as PSs due to their versatile physicochemical, photophysical and photochemical properties, which make them well-suited for applications in bioimaging and PDT.[13,14,24–26] Compared to traditional organic PSs, metal complexes offer several distinct advantages. As previously mentioned, the presence of a heavy metal atom enhances SOC, thereby facilitating ISC to long-lived triplet excited states and improving the efficiency of ROS generation. Additionally, their robust photostability enables sustained ROS production at low doses, which helps minimize systemic toxicity and post-treatment photosensitivity. Furthermore, the modular architecture of these complexes allows for precise tuning of their photochemical behavior and biological interactions through strategic selection of metal centers and ligands. Despite the growing interest in metal-based PSs, comprehensive reviews specifically addressing the development and mechanistic understanding of type I photoreactivity in these systems remain surprisingly limited.

Here, we highlight key design strategies—such as cyclometalation with thiophenyl-based ligands, conjugation with organic fluorophores like coumarin or BODIPY, and the development of multinuclear architectures—that have been investigated to enhance electron-transfer reactivity under hypoxic conditions.

3.1. Bis-cyclometalated iridium(III) complexes: synergistic type I/II photosensitization

Cyclometalated Ir(III) complexes have emerged as versatile platforms for PDT due to their excellent photophysical properties.[27] Iridium(III) complexes distinguish themselves from organic fluorophores through the strong spin–orbit coupling of the metal center ($\xi = 3909$ cm^{-1}), which promotes efficient ISC to the triplet state. This results in long-lived excited states, often accompanied by high phosphorescence quantum yields. Their capacity to transfer energy to molecular oxygen and participate in photoredox processes makes them excellent candidates for both type I and type II photodynamic mechanisms.[28] In addition, their large Stokes' shifts, emission in the visible to near-infrared (NIR) region, and high photostability make them particularly suitable for combined imaging and therapeutic applications.[29]

In our initial investigation of Ir(III) complexes for PDT, we reported a series of 2-(thiophen-2-yl)benzimidazole-based cyclometalated Ir(III) complexes (**Ir1–3**; Fig. 2) containing dipyrido[3,2-a:2′,3′-c]phenazine (dppz) as N^N ligand that exhibited dual type I/II photoreactivity under normoxic conditions (21% O$_2$). Notably, under hypoxic conditions (2% O$_2$)—mimicking the tumor microenvironment—their photoreactivity shifted predominantly

toward a type I mechanism, producing superoxide radicals with minimal singlet oxygen generation. This behavior highlights a key feature of these compounds: their environmental adaptability. Upon blue-activation (1 h, $\lambda_{max} = 420$ nm, 77 ± 3 W m^{-2}), the compounds induced effective cell killing in HeLa cells, with phototoxicity indexes (PIs) exceeding 40 in hypoxia.[30]

A second-generation series of bis-cyclometalated Ir(III) dppz complexes incorporating 2-(5-aryl-thienyl)-benzothiazole ligands, was designed to shift the absorption bands toward the more tissue-penetrating region of the visible spectrum.[31] The chromophoric nature of 2-(5-arylthiophen-2-yl)benzothiazole, featuring an electron-donating N,N-dimethylaminophenyl ring connected to an electron-withdrawing benzothiazole moiety in **Ir4** (Fig. 3), enabled a red-shifted absorption profile with bands around 500 nm and tails extending to 620 nm. **Ir4** was capable of photocatalytically oxidizing NADH under blue light irradiation and generating ^{1}O$_2$ and •OH in cell-free media. The complex showed minimal dark toxicity and high phototoxicity upon blue light irradiation (PI > 71). Remarkably, **Ir4** could also be activated by green and red light, albeit with reduced efficacy. Park et al. reported neutral Ir(III) complexes (**Ir5** and **Ir6**; Fig. 3) featuring thiophene-based cyclometalating ligands and a morpholine moiety for lysosome-targeting.[32] Upon white-light irradiation (0.6 J cm^{-2}), **Ir5** generated both singlet oxygen and radical species (•O$_2^-$ and •OH), indicating a dual type II and type I photoreactivity mechanism. Notably, **Ir5** and its analogue **Ir6** preferentially accumulated in lysosomes, where protein oxidation disrupted lysosomal membrane integrity and disrupted autophagic flux. In 2D cancer cell models, both complexes exhibited enhanced PDT efficacy, even under drug-resistant conditions. Proteomic analyses suggested that the therapeutic effect was linked to spatiotemporal protein oxidation within lysosomes, identifying autophagy as a vulnerable pathway. Furthermore, the red-light activatable analogue **Ir6** demonstrated strong in vivo efficacy against drug-resistant tumors, underscoring the translational potential of that approach.

A structurally related Ir(III) complex (**Ir7**; Fig. 3), reported by Zhu and co-workers,[33] showed strong phototoxicity under green-light irradiation (525 nm, 100 mW cm^{-2}, 5 min), with IC$_{50}$ values as low as 91 nM in 4T1 breast cancer cell line. Spectroscopic and computational analyses confirmed its ability to produce both singlet oxygen and superoxide radicals, supporting a combined type II/type I photoreactivity profile. Beyond efficient ROS production, **Ir7** activated a distinct cell death pathway: ferroptosis. Using GPX4-overexpressing and GPX4-knockout cell models, the authors demonstrated that **Ir7** not only induces lipid peroxidation via ROS-mediated oxidative stress but also directly impairs glutathione metabolism and GPX4 activity. This dual mode of action amplifies oxidative imbalance and promotes ferroptotic cell death, contributing to **Ir7**'s remarkable antitumor efficacy, as validated by in vivo by tumor growth inhibition.

Building upon the thiophenyl scaffold, two subsequent studies from our group explored the incorporation of (thiophenyl)benzimidazole ligands into Ir(III) complexes, with a rational design aimed at enhancing selective tumor accumulation
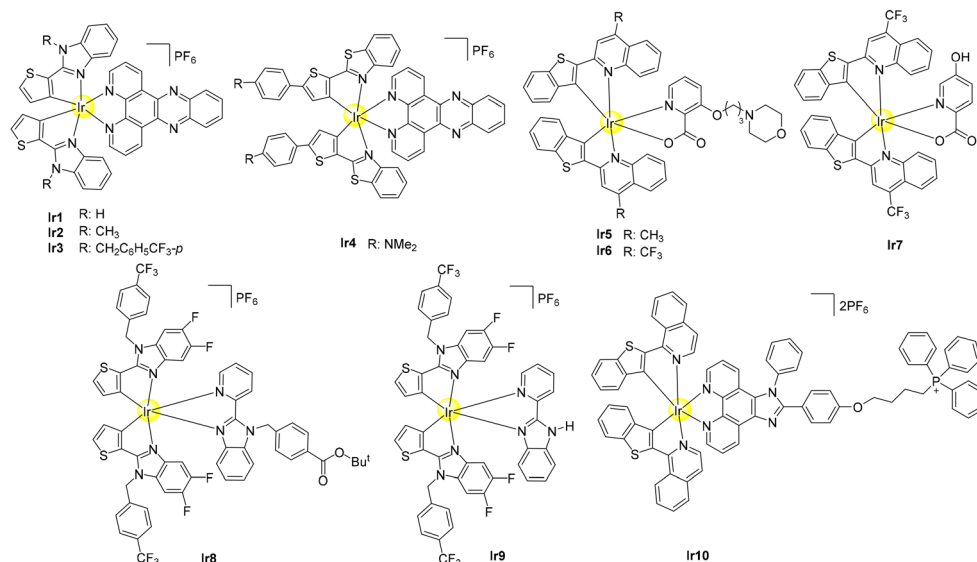
Fig. 3   Thiophenyl-based cyclometalated Ir(III) PSs.

through strong and specific binding to human serum albumin (HSA).[34,35] In the first approach, theoretical calculations guided the design of [Ir(5,6-difluoro-2-(thiophen-2-yl)-1-(4-(trifluoromethyl)benzyl)-1H-benzo[d]-imidazole)$_2$(tert-butyl 4-((2-(pyridin-2-yl)-1H-benzo[d]-imidazole-1-yl)methyl)benzoate)]$^+$ (**Ir8**, Fig. 3), which exhibited high-affinity interaction with HSA.[34] This resulted in a significant increase in protein binding capacity, promoting passive tumor targeting via the enhanced permeability and retention (EPR) effect. A second strategy involved the direct conjugation of **Ir9** (Fig. 3) to HSA, yielding a robust biomolecular assembly with improved aqueous solubility and enabling oncosis-mediated PDT.[35] Both systems retained strong photobiological activity under blue-light irradiation (450 nm, 1.2 J cm^{-2}), efficiently oxidizing NADH and generating singlet oxygen through combined type I/type II mechanisms. In vitro studies against colon cancer cells (CT-26) revealed high photocytotoxicity (PI = 34–89), with negligible dark toxicity.

Chen and co-workers reported a mitochondria-targeting Ir(III) PS functionalized with a triphenylphosphonium group (**Ir10**; Fig. 3), enabling simultaneous mitochondrial modulation of macrophages and cancer cells to achieve synergistic antitumor immunity.[36] Under white light irradiation (6 mW cm^{-2}, 15 min), **Ir10** generated $^1O_2$, $^\bullet O_2^-$ and $^\bullet OH$ in mononuclear macrophage leukemia RAW264.7 cells, confirming its dual type II/type I photoreactivity in vitro. **Ir10** exhibited higher phototoxicity toward 4T1 tumor cells (PI > 145) than toward macrophages (PI > 48), attributed to differences in cellular uptake. Mitochondrial targeting also enhanced **Ir10**'s ability to induce immunogenic cell death (ICD) in 4T1 cells. Remarkably, **Ir10** demonstrated good PDT efficacy in vivo and effectively activated a systemic immune response with favorable biosafety.

To address the limited tissue penetration of blue light and red-shift the absorption wavelength of Ir(III) complexes,[37] we designed an Ir-coumarin conjugate (**Ir-COUPY-1**, Fig. 4) that can be activated with green light, thanks to the coumarin moiety, while retaining its ability to generate radicals.[38] The compound exhibited no dark cytotoxicity (IC$_{50}$ > 200 μM) in HeLa cells. Notably, under low doses of green light (21 J cm^{-2}), the IC$_{50}$ value dropped to 2.51 μM, resulting in a PI of 85. The Ir(III)-COUPY conjugate maintained high photocytotoxicity under hypoxic conditions (2% O_2), with a hypoxia index (HI) close to 1. This index, defined as the ratio of light IC$_{50}$ in normoxia to light IC$_{50}$ in hypoxia, provides an idea of the potency of a PS under oxygen-deficient conditions. The use of various ROS scavengers confirmed that the primary ROS generated by **Ir-COUPY-1** was $^\bullet O_2^-$, positioning it as a promising type I PS.[39]

To investigate structure–activity relationships (SAR), a series of Ir(III)-COUPY conjugates (**Ir-COUPY-2–5**, Fig. 4) were synthesized to explore how structural modifications within the COUPY unit influence ROS generation and photocytotoxicity.[40] The absence of the N,N-diethylamino electron-donating group (EDG) in **Ir-COUPY-2** caused a pronounced blue-shift in absorption and abolished both ROS generation and photocytotoxicity, highlighting the critical role of the EDG at position 7 of the coumarin backbone in photoreactivity. In contrast, the julolidine-fused analogue **Ir-COUPY-3** exhibited red-shifted absorption and emission, but required higher intracellular accumulation to achieve cytotoxic effects, indicating reduced photoreactivity. Conjugates **Ir-COUPY-4** and **5**, which incorporated longer linkers while retaining the COUPY core of **Ir-COUPY-1**, displayed similar photophysical properties and ROS production, but showed enhanced phototoxicity under hypoxia. **Ir-COUPY-1**, **-4**, and **-5** induced potent cell death via ROS-mediated necrosis under green light irradiation, even in hypoxic and cisplatin-resistant models, with strong inhibition also observed in 3D tumor spheroids. Overall, these findings underscore the importance of precise structural tuning of the COUPY scaffold to optimize type I ROS generation and phototherapeutic efficacy under clinically relevant conditions.
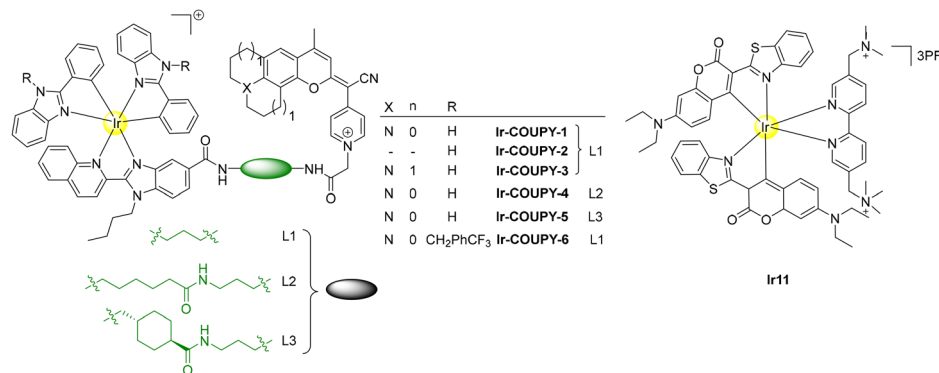
Fig. 4   Ir(III)-coumarin PSs.

Building on previous strategies aimed at tuning photoreactivity through coumarin and linker modifications, a subsequent strategy focused on reengineering the cyclometalated Ir(III) scaffold itself. The incorporation of trifluorobenzyl substituents into the cyclometalating ligand of the Ir(III) complex led to the development of **Ir-COUPY-6** (Fig. 4),[41] a conjugate exhibiting significantly enhanced photophysical properties, including stronger absorption and improved luminescence. Importantly, **Ir-COUPY-6** exhibited potent photocytotoxicity under red-light irradiation (620 nm), efficiently generating both type I and II ROS—even under hypoxic conditions—while maintaining minimal dark toxicity. Compared to earlier analogues, its superior performance under red light resulted into higher PI values and deeper tissue penetration, key advantages for the treatment of solid tumors. Beyond $^{\bullet}O_2^-$ photogeneration, **Ir-COUPY-6** also produced $^{\bullet}OH$ and catalyzed NADH oxidation under hypoxia. Density functional theory (DFT) calculations supported a photoinduced electron transfer from the coumarin moiety to the Ir(III) complex, favoring superoxide formation and reinforcing its type I mechanism. Taken together, these findings demonstrate that fine-tuning the conjugation between COUPY dyes and rationally designed Ir(III) complexes, represents a powerful strategy for developing red-light activated type I PSs with robust activity under low-oxygen conditions.

Other Ir-coumarin PSs have also proven effective under hypoxic conditions *via* a type I mechanism.[42–45] For example, Huang *et al.* developed an Ir(III)-coumarin complex (**Ir11**, Fig. 4) bearing a C^N coumarin-6-based ligand and a quaternized bipyridine (4,4′-bis(*N*,*N*,*N*-trimethylmethanaminium)-2,2′-bipyridine) as the N^N ligand.[42] This structural modification rendered **Ir11** water-soluble and enabled efficient photocatalytic activity through a single-electron transfer (SET) mechanism. Upon blue light irradiation (465 nm, 11.7 J cm^{-2}), **Ir11** promoted the oxidation of NAD(P)H and amino acids, consistent with type I reactivity, and displayed strong photocytotoxicity against various cancer cell lines while remaining non-toxic in the dark (PI: 40–172). Notably, **Ir11** also showed significant antitumor efficacy *in vivo*, effectively inhibiting tumor growth in both zebrafish and murine models upon light activation, further supporting its potential as a type I PDT agent in biologically relevant hypoxic environments.

Although coumarin-based PSs can be structurally tuned to absorb light in the visible and even far-red region,[46] their absorption bands are generally narrower than those of phthalocyanines (Pcs), which inherently exhibit intense and broad absorption in the far-red to NIR region. In this context, the Ir(III)-phthalocyanine conjugate (**Ir12**, Fig. 5)[47] showed strong absorption at 677 nm and improved photostability compared to free ZnPc. When encapsulated in polyurethane-polyurea hybrid nanocapsules, **Ir12** exhibited high photocytotoxicity under 630 nm light irradiation in both normoxic and hypoxic conditions, attributed to its dual type I and type II ROS generation. It also demonstrated excellent phototherapeutic efficacy in 3D tumor spheroid models. These results illustrate an alternative design strategy for red-light-activated PSs, offering a complementary approach to coumarin-based systems.

Boron dipyrromethene (BODIPY) fluorophores have been also introduced into iridium complexes for achieving long-wavelength absorption. For example, Chao *et al.*[48] reported an **Ir-BODIPY-1** conjugate (Fig. 5) with an intense absorption in the green region (λ_{abs} = 500 nm) that can generate both type I/type II ROS ($^1O_2$, $^{\bullet}OH$, and $^{\bullet}O_2^-$). **Ir-BODIPY-1** was highly photoactive against triple-negative breast cancer cells with PI values ranging from 172 to 519 under a moderate flux of visible-light irradiation (500 nm, 10.5 mW cm^{-2}). Remarkably, the antiproliferative activity of **Ir-BODIPY-1** was retained under hypoxic conditions (2.5% O$_2$). Very recently, Su *et al.* designed a type-I **Ir-BODIPY-2** conjugate (Fig. 5) by modulating the triplet state energy through ligand engineering.[49] To achieve this, they performed time-dependent density-functional theory (TDDFT) calculations comparing two cyclometalating ligands: 2-phenyl-pyridine (ppy) and 2-phenylbenzo[*d*]thiazole (bpt). The ppy-based conjugate exhibited a triplet-to-ground state energy gap ($\Delta E_{T_1-S_0}$) of 1.674 eV, sufficient to overcome the energy barrier between $^3O_2$ and $^1O_2$ (1.61 eV), thereby enabling efficient $^1O_2$ generation under irradiation. In contrast, **Ir-BODIPY-2** containing the bpt ligand reduced the $\Delta E_{T_1-S_0}$ to 1.425 eV, which suppressed energy transfer and favored an electron transfer pathway, effectively converting a type II PS into a type I. Extracellular and intracellular experiments confirmed the production of $^{\bullet}OH$ and $^{\bullet}O_2^-$, rather than $^1O_2$ for **Ir-BODIPY-2** upon red laser irradiation (630 nm, 0.6 W cm^{-2}, 5 min) under hypoxic conditions. Moreover, irradiation severely disrupted the intracellular photoredox balance, triggering pyroptosis, a form of programmed cell death. RNA sequencing and *in vivo*
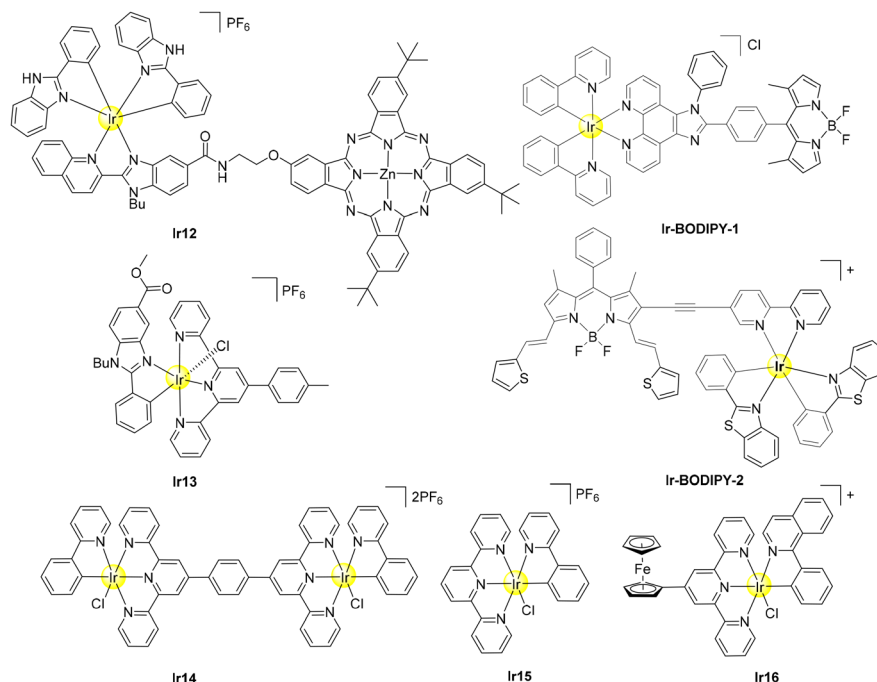
Fig. 5 Examples of Ir(III)-based PSs.

experiments further demonstrated that **Ir-BODIPY-2** effectively induced ICD and suppressed solid tumor growth. This study demonstrates the importance of rational structural design in advancing cancer phototherapy.

Inspired by the work of Sadler *et al.* on an iridium complex bearing a terpyridine ligand that exhibits phototoxicity toward both normoxic and hypoxic cancer cells,[50] we developed a series of Ir(III) complexes incorporating the terdentate ligand 4′-(*p*-tolyl)-2,2′:6′,2′′-terpyridine (ttpy), and a C^N ligand derived from a deprotonated 2-arylbenzimidazole backbone.[51] Under blue light irradiation, these iridium complexes efficiently mediate the photooxidation of NADH and generate $^1O_2$ and $^\bullet OH$ *via* a combined type I/II mechanism. To assess their potential for treating brain tumors, we evaluated their ability to cross the blood–brain barrier using a range of *in vitro* models. Among the series, the complex **Ir13** (Fig. 5), which features a deprotonated methyl 1-butyl-2-phenylbenzimidazolecarboxylate ligand, emerged as a particularly promising candidate for targeting therapy-resistant brain tumors. Upon blue laser irradiation (405 nm, 60 s, 1 mW), **Ir13** triggers a rapid and sustained ROS-induced cytotoxic response and shows preferential accumulation in tumor tissues. These properties highlight its potential for fluorescence-guided PDT in combination with surgical resection of glioblastoma. Remarkably, **Ir13** also displayed tumor-suppressing activity in the absence of light, outperforming standard temozolomide treatment while sparing healthy brain tissue.

Huang *et al.* also developed Ir(III) photocatalysts bearing tridentate ligands that exhibit synergistic type I/II photosensitization and photocatalytic activity.[52,53] For instance, the dinuclear Ir(III) complex (**Ir14**, Fig. 5) showed a markedly enhanced photocatalytic oxidation of NAD(P)H—up to 13-fold greater than its mononuclear analogue **Ir15**—demonstrating a clear

synergistic effect between the two metal centers. **Ir14** also catalyzed the oxidation of amino acids such as proline and tryptophan, along with H_2O_2 generation, contributing to its potent photoactivated anticancer activity in various cell lines and *in vivo* models. Notably, **Ir14** exhibited superior photocytotoxicity under green light irradiation (525 nm; 29.56 J cm^{-2}) in HepG2 cells (PI = 660), likely due to its enhanced light absorption and higher intracellular ROS generation. Its lysosomal localization and favorable biocompatibility further improved its therapeutic performance. This study also introduced the use of single-cell ICP-MS to quantify iridium uptake at the cellular level—marking the first application of this technique to evaluate the intracellular distribution of metal-based PSs.

More recently, Chao *et al.* reported a photoactivated ferrocene-iridium(III) complex with a tridentate ligand designed to overcome drug resistance in melanoma by disrupting cancer stem cell properties and inducing ICD.[54] Upon blue light irradiation (405 nm, 20 mW cm^{-2}, 600 s), **Ir16** (Fig. 5) undergoes cleavage, releasing Fe^{2+} ions and a cytotoxic Ir-based PS. This dual-action mechanism enables the generation of both $^\bullet OH$ and $^\bullet O_2{}^-$ radicals—even under hypoxic conditions—triggering ferroptosis, autophagy, and ICD. To enhance tumor selectivity and biocompatibility, **Ir16** was encapsulated in DSPE-PEG2000 nanoparticles (**Ir16@PEG**), which showed improved accumulation in tumor tissue after systemic administration. Light activation of **Ir16@PEG** significantly downregulated stemness markers and inhibited the growth of both primary and distant melanoma tumors *in vivo*.

3.2. Ruthenium(II) complexes: type I performance through cyclometalation

Ru(II) complexes have gained significant attention for their potential applications in PDT.[55–57] A notable example is the

Ru(II) complex **TLD-1433**, which has advanced to Phase II clinical trials for the treatment of non-muscle-invasive bladder cancer using irradiation with green light.[58] Ru-based compounds exhibit several advantageous properties, including high photostability, partially filled d orbitals, and higher molar extinction coefficients in the visible range compared to Ir complexes. Moreover, their ability to adopt multiple oxidation states enable diverse redox reactions, making them particularly versatile for type I photodynamic processes.

Although most Ru-based PSs described in the literature primarily rely on N^N ligands,[59–61] several research groups—including ours—have explored the incorporation of cyclometalated C^N ligands as a rational strategy to address the challenges posed by the hypoxic tumor microenvironment. These ligands, owing to their electron-donating nature, can modulate the electronic structure of the metal center by raising the energy of the $d\pi$(Ru) orbital, resulting in a cathodic shift of the Ru(II/III) redox potential.[62,63] This electronic tuning favors electron transfer over energy transfer processes, thereby facilitating the generation of ROS through a type I mechanism.[64] In addition, the anionic character of the C^N ligand induces a bathochromic shift of the metal-to-ligand charge transfer (MLCT) absorption band of the Ru(II) cyclometalated complex.[65–67]

In 2016, McFarland *et al.* reported the first class of potent light-responsive cyclometalated Ru(II) complexes.[62] They investigated how π-expansive cyclometalating ligands influence the photophysical and photobiological properties of organometallic Ru(II) compounds. Among them, **Ru1**—featuring the most π-expansive cyclometalating ligand—exhibited red-shifted absorption and low singlet oxygen quantum yield compared to its Ru(II) polypyridyl counterpart. Notably, **Ru1** was non-toxic in the dark ($IC_{50} > 300 \mu M$) but showed nanomolar range phototoxicity, attributed to intracellular generation of $^{\bullet}O_2^-$ under visible-light irradiation (50 J cm^{-1}).

The same group later designed and synthetized a new class of cyclometalated Ru(II) complexes incorporating π-extended benzo[*h*]imidazo[4,5-*f*]quinoline (IBQ) cyclometalating ligands. **Ru2**, the Ru(II) C^N analog of **TLD-1433**,[67,68] was cytotoxic to SK-MEL-28 melanoma cells in the dark but showed selective toxicity toward cancer cells over normal skin fibroblasts, suggesting its potential as a selective chemotherapeutic agent. In contrast, **Ru3**—bearing an additional thienyl group appended to the IBQ ring—was non-toxic to melanoma cells in the dark and exhibited a high PI (>1400) under visible-light irradiation. **Ru3** also showed a low singlet oxygen quantum yield (16%), suggesting that its photodynamic activity may arise from a dual type II/type I mechanism.

A family of heteroleptic complexes of the general formula [Ru(C^N)(N^N)₂][PF₆] (HC^N = methyl 1-butyl-2-arylbenzimidazolecarboxylate; N^N = polypyridine) was synthesized to serve as biologically-compatible PSs activated by green light.[69] Under low doses of green light (1 h, 1.3 mW cm^{-2}), **Ru4** and **Ru5** (Fig. 6) exhibited the highest PI values, with **Ru4** exceeding 750 in HeLa and A2780cis cancer cells, and displaying nanomolar IC_{50} values. Notably, both complexes were active under both normoxic and hypoxic conditions. In normoxia, H_2O_2 was

identified as the primary photogenerated species, although other ROS such as $^{\bullet}OH$ or $^1O_2$ were also produced. Under hypoxic conditions, **Ru4** and **Ru5** retained the ability to photogenerate H_2O_2 and $^{\bullet}O_2^-$ species, indicating a preference for type I photodynamic mechanism at low oxygen concentrations.

A new generation of cyclometalated Ru(II) polypyridyl complexes was rationally designed and synthesized.[70] The incorporation of an electron-withdrawing substituent (CF₃) in the position 3 of the phenyl ring in the cyclometalating ligand (Fig. 6) was carried out to investigate their influence on the complexes' absorption properties and photobiological activities. These Ru complexes exhibited absorption maxima around 560 nm, with a tail extending up to 700 nm. In free-cell media, the compounds were capable of generating $^1O_2$ upon green light irradiation ($\lambda = 520$ nm) in acetonitrile, with **Ru6** containing dipyrido[3,2-*d*:2′,3′-*f*]quinoxaline (dpq) as N^N ligand and **Ru7** with bipyridine (bpy), showing the highest performance ($^1O_2$ quantum yields of 0.15). In addition, **Ru6** and **Ru7** were also able to photogenerate $^{\bullet}OH$, demonstrating the ability to operate *via* both type I and type II PDT mechanisms. Under irradiation with green light (545 nm, 1 h, 22 W m^{-2}), the complexes also produced ROS at the cellular level. Upon illumination, **Ru6** was able to disrupt phospholipid membranes and induce mitochondrial membrane depolarization.

A series of octahedral Ru(II) complexes with the general formula [Ru(C^N)(phen)₂]$^+$ incorporating π-extended cyclometalated benzo[*g*]quinoxaline ligands (C^N) and phenanthroline co-ligands, were developed and evaluated for their anticancer phototherapeutic properties.[71] These complexes demonstrated notable light-induced cytotoxicity in human cervical, melanoma, and colon cancer cell lines, particularly under blue light irradiation. Among them, **Ru8** (Fig. 6) exhibited the highest potency, achieving PI values up to 100 in HCT116 colon cancer cells. This activity was attributed to its ability to generate singlet oxygen and hydroxyl radicals *via* a dual type I and type II mechanism. Cellular studies revealed that **Ru8** predominantly localizes in to cellular membranes and, upon photoactivation, induces lipid peroxidation *via* ROS generation. This oxidative damage compromises membrane integrity, activates caspase-3, and initiates apoptosis, supporting a membrane-targeted PDT mechanism. Notably, **Ru8** also exhibited the ability to eradicate colon cancer stem cells, a subpopulation often linked to treatment resistance, recurrence, and metastasis.

Building on the promising performance of Ir(III)-COUPY conjugates under hypoxic conditions, a Ru(II)-COUPY complex was rationally designed to integrate red/NIR absorption with dual type I and II photoreactivity.[72] In this construct, a julolidine-fused CF₃-coumarin was conjugated to a Ru(II) polypyridyl complex bearing two dipyrido[3,2-*d*:20,30-*f*]quinoxaline (dpq) ligands and a benzimidazole-based C^N ligand. The resulting **Ru-COUPY** conjugate (Fig. 7) showed far-red/NIR absorption and emission (626/698 nm), improved photostability, and cellular selectivity. It was capable of generating both $^1O_2$ and $^{\bullet}O_2^-$ under green and red light irradiation, even under hypoxic conditions. Compared to its individual components, **Ru-COUPY** displayed negligible dark toxicity ($IC_{50} > 300 \mu M$)
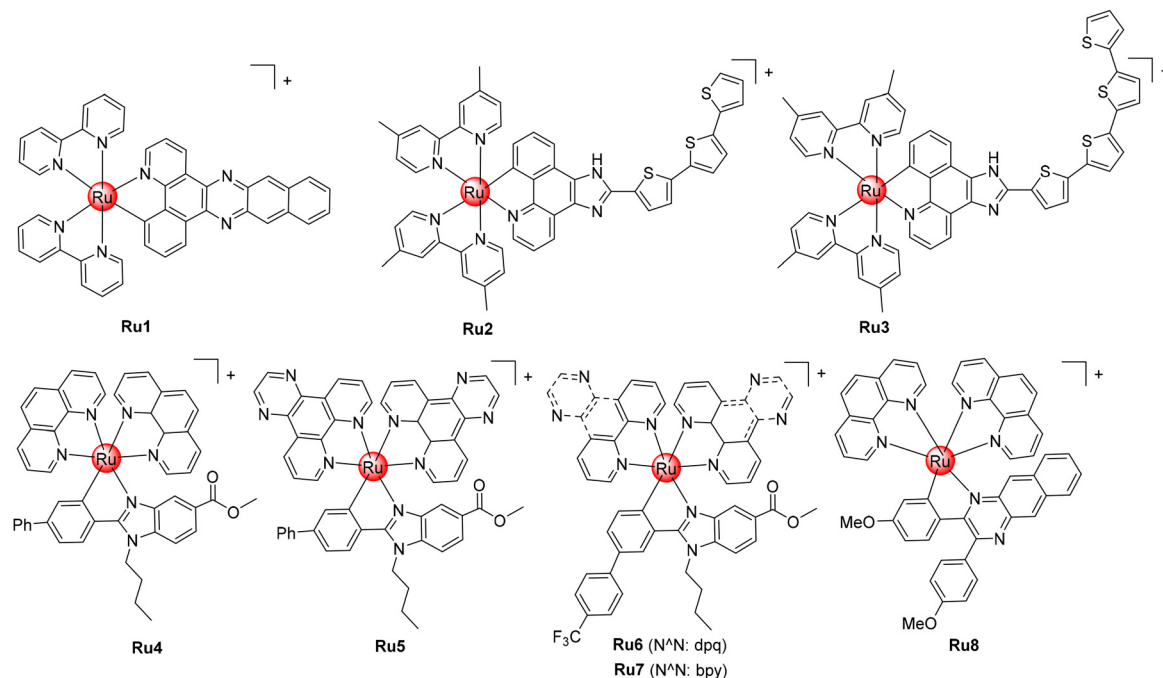
Fig. 6 Examples of cyclometalated Ru(II)-based PSs.

and superior phototoxicity, achieving a PI > 300 in CT-26 cells under 620 nm light, while retaining activity up to 740 nm.

Huang *et al.* developed a type I PS based on cyclometalated Ru(II) complex incorporating a coumarin moiety into the cyclometalated ligand (2-(3,4-difluorophenyl)pyridine) (**Ru9**, Fig. 7).[64] **Ru9** showed enhanced visible light absorption compared to the free coumarin. Upon white light irradiation (10 min), **Ru9** demonstrated enhanced efficacy under both normoxic and hypoxic conditions, reducing cell viability to 3.1% at 20 μM. **Ru9** maintained the activity even under hypoxic conditions,

which was attributed to the generation of highly oxidative hydroxyl radicals *via* a type I photochemical mechanism. Moreover, *in vivo* studies in tumor-bearing mice confirmed the antitumor efficacy of **Ru9**, showing significant inhibition of tumor growth upon light irradiation.

Expanding on the success of Ir/Ru-COUPY conjugates, where coumarin dyes are appended to the metal scaffold *via* nonconjugated linkers, we recently introduced a structurally distinct design strategy involving direct conjugation of the fluorophore to a ligand through a π-conjugated linker. This
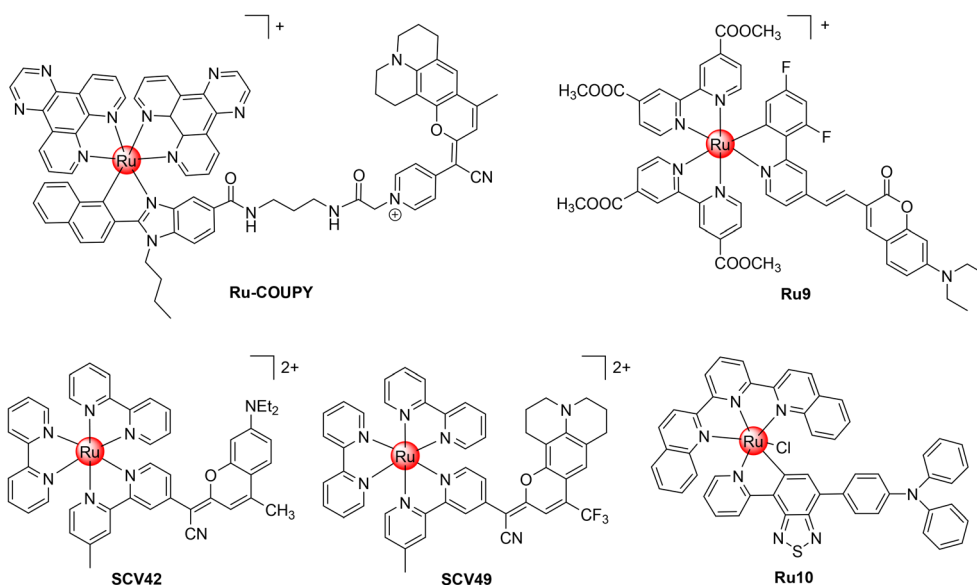

Fig. 7 Ru(II)-coumarin and Ru(II)-TPABP PSs.

approach enabled the development of a new family of Ru(II)-based PSs (**SCV42**, **SCV49**, Fig. 7) incorporating COUPY-derived 2,2′-bipyridyl ligands (COUBPYs).[73] These complexes display strong absorption in the visible region, extending up to the NIR in some cases, thereby allowing efficient photoactivation with green, red, and NIR light. Photochemical studies using fluorogenic probes and electron spin resonance (ESR) spectroscopy revealed that Ru-COUBPY complexes generate both type I (superoxide, hydroxyl radical) and type II (singlet oxygen) ROS, while retaining high phototoxicity under hypoxic conditions. Among them, **SCV49** emerged as the lead candidate, displaying nanomolar photocytotoxicity and PI values exceeding 30 000 in CT-26 cells under deep-red light irradiation. *In vivo* PDT efficacy studies in murine subcutaneous tumor models of colorectal cancer confirmed the therapeutic potential of **SCV49**, demonstrating excellent tolerability and strong tumor growth inhibition upon irradiation with deep-red light (660 nm). These results position **SCV49** as a highly promising hypoxia-active PS for advanced anticancer PDT.

Very recently, Sun *et al.* have reported cyclometalated NIR-absorbing Ru-based PSs capable of type I photoreactivity.[74] The cyclometalated Ru enantiomers (Λ/Δ-**Ru10**, Fig. 7), [Λ/Δ-Ru-dqpy-TPABP]Cl (dqpy = 2,6-di(quinolin-2-yl)pyridine; TPABP = 4-(4-(pyridine-2-yl)-2,1,3-benzothiadiazol-7-yl)triphenylamine), exhibited strong metal- and ligand-to-ligand charge transfer (ML-LCT) absorption around 640 nm with an extended tail reaching 800 nm. The electron-rich TPABP ligand facilitates triplet-state formation and enhances electron transfer, promoting type I ROS generation and effective phototoxicity under hypoxic conditions. Encapsulation into polymeric nanoparticles further improves tumor-targeted delivery, resulting in high inhibition of primary tumors ($>85\%$) and suppression of breast tumor lung metastases under 700 nm light irradiation. This work highlights how rational design of cyclometalating ligands can enable NIR-active Ru PSs for type I PDT applications.

4. Challenges in the experimental identification of type I mechanisms and their biological evaluation

Despite the increasing relevance of type I photochemical pathways in PDT, the field still lacks standardized and unequivocal methodologies for their experimental identification. Many commonly used ROS detection techniques remain qualitative and are often influenced by the biological context, limiting their reliability. For example, dihydrorhodamine 123 (DHR123) is frequently employed to detect $^{\bullet}O_2^-$ in cell-free systems, as it undergoes oxidation to fluorescent rhodamine 123. However, in cellular environments, this oxidation can also be mediated by H_2O_2 in the presence of endogenous peroxidases,[75] thereby compromising its specificity for superoxide in live-cell assays. In contrast, dihydroethidium (DHE)[76] is better suited for superoxide detection within cells, as its oxidation product binds to DNA, producing a strong fluorescent signal. Nevertheless, this DNA-binding requirement makes DHE unsuitable for cell-free systems.

ESR spectroscopy remains the most direct and informative technique for detection and characterization of ROS, particularly when combined with spin trapping agents.[77] The most widely used spin trap for superoxide is 5,5-dimethyl-1-pyrroline *N*-oxide (DMPO), which forms a stable adduct with $^{\bullet}O_2^-$ in methanolic solutions, yielding a characteristic ESR signal with a peak integral ratio of 1:1:1:1. However, in aqueous media, DMPO can also trap $^{\bullet}OH$,[12] forming a DMPO–$^{\bullet}OH$ adduct with a distinct 1:2:2:1 signal pattern, which often exhibit short half-lives that can compromise signal stability and lead to potential inaccuracies in ROS identification. To overcome this, improved spin traps such as 5-diethoxyphosphoryl-5-methyl-1-pyrroline *N*-oxide (DEPMPO) and 5-*tert*-butoxycarbonyl-5-methyl-1-pyrroline *N*-oxide (BMPO)[78] have been developed, offering extended adduct stability and enhanced accuracy in distinguishing between superoxide and hydroxyl radical formation.

Among the type I ROS, $^{\bullet}OH$ is considered the most reactive and cytotoxic. Its detection is commonly achieved using 3-(*p*-hydroxyphenyl) fluorescein (HPF), a fluorogenic probe that reacts specifically with $^{\bullet}OH$, resulting in the release of fluorescein with bright green emission. This reaction occurs with minimal interference from other ROS, such as singlet oxygen or superoxide, making HPF a preferred a simple method for detecting hydroxyl radicals in both *in vitro* and non-cellular contexts. Regardless of the probe used, it is crucial to include parallel controls with ROS scavengers—such as superoxide dismutase (SOD) for $^{\bullet}O_2^-$ or mannitol for $^{\bullet}OH$ to confirm the identity of the ROS and avoid false-positive signals.

Together, these methods provide valuable insight into the types of ROS generated during PDT. However, results should be interpreted with caution and, ideally, multiple approaches should be combined to strengthen mechanistic conclusions. As emphasized in the guidelines proposed by Li *et al.*,[12] the inclusion of appropriate controls (*e.g.*, ROS scavengers, hypoxic conditions, light-only *vs.* dark treatments) is essential to validate whether ROS production arises from type I photochemical pathways. It is also worth noting that many ROS probes and ESR spin-trapping techniques suffer from limited selectivity and may yield overlapping or misleading signals. Therefore, rigorous cross-validation using independent detection methods is essential to draw robust mechanistic conclusions.

In addition to direct ROS detection, monitoring the photooxidation of NADH to NAD$^+$ has become a widely used strategy to probe potential type I photoreactivity in metal-based PSs. However, the mechanistic interpretation of this assay remains under active debate. Recent studies have framed this process within the broader context of photocatalytic cancer therapy, rather than strictly as type I PDT.[79,80] A key point of debate is whether the NADH oxidation is directly mediated by the excited PS *via* a photoinduced electron transfer (PET) mechanism, or indirectly driven by ROS (*e.g.*, $^{\bullet}OH$, $^1O_2$, or $^{\bullet}O_2^-$) generated during the photodynamic process. Nonetheless, previous mechanistic studies have demonstrated that NADH photooxidation can proceed *via* a single electron transfer (SET) from

NADH to the triplet excited state of the metal complex, forming highly reactive $PS^{\bullet-}$ and $NAD^{\bullet}$ intermediates.[50] Under oxygen-depleted conditions, this reaction is typically attenuated but not entirely suppressed, supporting the involvement of a type I pathway.[35,81] According to the proposed type I catalytic cycle, the $PS^{\bullet-}$ species reacts with molecular oxygen to regenerate the ground-state complex and produce $^{\bullet}O_2^{-}$. These radicals can further react with $NAD^{\bullet}$ intermediates to ultimately yield NAD^{+} and H_2O_2, thereby completing the redox cycle.[35] This mechanistic duality raises an important conceptual question: should NADH photooxidation be considered a hallmark of canonical type I PDT, or rather part of a broader photocatalytic paradigm that also encompasses the emerging type III pathway, in which PSs directly oxidize biomolecules in a largely ROS-independent fashion? Regardless of terminology, the assay provides valuable mechanistic insights, but robust classification requires complementary ROS detection, scavenger controls, and hypoxia studies.

Moreover, the photochemical processes underlying type I mechanisms in complex biological environments remain insufficiently characterized, particularly regarding the dynamic interactions between PSs and diverse biomolecules within the cellular microenvironment. Identifying their intracellular targets and rationally designing PSs that selectively oxidize key biomolecular components[50]—such as membrane lipids, proteins, or nucleic acids—remains a significant and unresolved challenge.[5] In addition, most mechanistic studies rely heavily on simplified 2D cell cultures or cell-free systems, which fail to fully recapitulate the complexity of the tumor microenvironment. There is a growing need to incorporate biologically relevant models, such as 3D spheroids,[82,83] to better assess oxygen gradients, ROS diffusion, and PS behavior under physiologically realistic conditions.

From a translational perspective, the absence of a predictable dose–response relationship in many biological models complicates the development of clinically viable therapies. Even when *in vitro* phototoxicity is demonstrated under normoxic and hypoxic conditions, these findings often fail to translate effectively *in vivo* due to factors such as limited PS accumulation, metabolic degradation, or heterogeneity within the tumor microenvironment.

5. Conclusions and outlook

Cyclometalated Ir(III) and Ru(II) complexes have emerged as highly promising platforms for the development of type I PSs. Their intrinsic heavy-atom effect, long-lived excited states, and tunable redox properties uniquely position them to facilitate electron or hydrogen transfer processes. These features enable sustained photoreactivity even under hypoxic conditions, which are characteristic of aggressive and treatment-resistant tumors.

From a molecular design perspective, the examples discussed herein underscore how subtle modifications to the cyclometalating ligands or the strategic incorporation of organic chromophores such as COUPY, phthalocyanine, and BODIPY, can significantly influence the photochemical behavior of these complexes. Such modifications allow for fine-tuning of the balance between type I and type II pathways, enabling dual photodynamic mechanisms and/or red-shift light activation. Notably, our group's contributions demonstrate that rational conjugation strategies not only extend absorption into the phototherapeutic window but also enhance photostability and performance in hypoxia—key attributes for therapeutic translation.

Despite these advances, several challenges persist in unequivocally identifying type I mechanisms and translating them into biological relevant environments. The limitations of conventional probes and assays, coupled with the lack of standardized protocols, often hinder accurate mechanistic elucidation. Furthermore, while promising results have been obtained in traditional 2D cell cultures, the transition to more physiologically relevant models—such as 3D spheroids and organoids—is imperative. These models better recapitulate the tumor microenvironment and are essential for establishing predictive structure–activity relationships that can guide therapeutic development.

Looking ahead, further exploration of ligand frameworks—such as COUBPYs—offers exciting opportunities to expand the type I reactivity landscape of iridium and ruthenium complexes.

However, achieving meaningful progress will require a more integrated approach that combines mechanistic insight with biological validation. This includes the development of improved photophysical and photochemical characterization methods, more robust biological evaluation platforms, and the design of PSs with enhanced selectivity and therapeutic efficacy. While molecular optimization of type I activity is clearly advancing, translating these developments into clinical practice requires careful consideration of practical constraints. Key factors include: (i) delivery and formulation strategies that ensure selective tumor accumulation while minimizing systemic photosensitivity; (ii) predictable pharmacokinetics and, where appropriate, rapid clearance; (iii) scalable and reproducible synthetic routes; and (iv) regulatory and safety evaluation frameworks that account for multimodal mechanisms of action (*i.e.* photochemistry combined with potential catalytic redox activity). To bridge promising *in vitro* findings with therapeutic translation, it is essential to incorporate clinically relevant endpoints into preclinical studies. These include testing in orthotopic models, conducting detailed toxicology and biodistribution analyses, and evaluating combination strategies with existing therapies.

Ultimately, the insights presented in this work aim to stimulate further innovation in the rational design of cyclometalated Ir(III) and Ru(II) complexes. By addressing current limitations and embracing interdisciplinary strategies, we can move closer to realizing oxygen-independent photodynamic therapies that are both effective and clinically viable.

Conflicts of interest

There are no conflicts to declare.

Data availability

No new data were generated in this review. All data presented are taken from previously published sources, as cited in the manuscript.

Acknowledgements

Notes and references

1 T. Hompland, C. S. Fjeldbo and H. Lyng, *Cancers*, 2021, **13**, 499.
2 Z. Chen, F. Han, Y. Du, H. Shi and W. Zhou, *Signal Transduction Targeted Ther.*, 2023, **8**, 70.
3 A. Sharma, J. F. Arambula, S. Koo, R. Kumar, H. Singh, J. L. Sessler and J. S. Kim, *Chem. Soc. Rev.*, 2019, **48**, 771–813.
4 H. D. Cole, J. A. I. Roque, G. Shi, L. M. Lifshits, E. Ramasamy, P. C. Barrett, R. O. Hodges, C. G. Cameron and S. A. McFarland, *J. Am. Chem. Soc.*, 2022, **144**, 9543–9547.
5 K.-X. Teng, L.-Y. Niu, J. Li, D. Zhang and Q.-Z. Yang, *Angew. Chem., Int. Ed.*, 2025, e202509416.
6 Y. Cai, T. Chai, W. Nguyen, J. Liu, E. Xiao, X. Ran, Y. Ran, D. Du, W. Chen and X. Chen, *Signal Transduction Targeted Ther.*, 2025, **10**, 115.
7 J. Li, Q. Yao, L. Wu, Z. Hu, B. Gao, X. Wan and Q. Liu, *Nat. Commun.*, 2022, **13**, 919.
8 S. Xu, Y. Yuan, X. Cai, C.-J. Zhang, F. Hu, J. Liang, G. Zhang, D. Zhang and B. Liu, *Chem. Sci.*, 2015, **6**, 5824–5830.
9 N. Ma, J. Wang, H. Tang, S. Wu, X. Liu, K. Chen, Y. Zhang and X. Yu, *Adv. Sci.*, 2025, **12**, 2413365.
10 J. Zhao, W. Wu, J. Sun and S. Guo, *Chem. Soc. Rev.*, 2013, **42**, 5323–5351.
11 M. Li, J. Xia, R. Tian, J. Wang, J. Fan, J. Du, S. Long, X. Song, J. W. Foley and X. Peng, *J. Am. Chem. Soc.*, 2018, **140**, 14851–14859.
12 M. Li, J. Xiong, Y. Zhang, L. Yu, L. Yue, C. Yoon, Y. Kim, Y. Zhou, X. Chen, Y. Xu, X. Peng and J. S. Kim, *Chem. Soc. Rev.*, 2025, **54**, 7025–7057.
13 Y. Wu, S. Li, Y. Chen, W. He and Z. Guo, *Chem. Sci.*, 2022, **13**, 5085–5106.
14 L. C.-C. Lee and K. K.-W. Lo, *Small Methods*, 2024, 2400563.
15 G. Vigueras and G. Gasser, *Nat. Chem.*, 2023, **15**, 896–898.
16 J. A. Roque, P. C. Barrett, H. D. Cole, L. M. Lifshits, G. Shi, S. Monro, D. von Dohlen, S. Kim, N. Russo, G. Deep, C. G. Cameron, M. E. Alberto and S. A. McFarland, *Chem. Sci.*, 2020, **11**, 9784–9806.
17 M. M. Alowakennu, A. Ghosh and J. K. McCusker, *J. Am. Chem. Soc.*, 2023, **145**, 20786–20791.
18 N. Sinha and O. S. Wenger, *J. Am. Chem. Soc.*, 2023, **145**, 4903–4920.
19 T. Sarkar, A. Bera, A. Upadhyay, N. Jain, V. Are, A. Eedara, R. D. Prakashchandra, S. Panneerselvam, J. B. Nanubolu, S. B. Andugulapati, S. Biswas and B. N. Babu, *ACS Appl. Mater. Interfaces*, 2025, **17**, 13660–13675.
20 L. Zhou, G. Salluce, P. Mesdom, M. Redrado, L. Gourdon-Grünewaldt, S. Hidalgo, O. Blacque, P. Arnoux, C. Frochot, K. Cariou and G. Gasser, *Inorg. Chem.*, 2025, **64**, 17058–17065.
21 D. Chen, Q. Xu, W. Wang, J. Shao, W. Huang and X. Dong, *Small*, 2021, 2006742.
22 C. Zhang, S. Hu, L. Jin, L. Lin, H. Lin, Z. Yang and W. Huang, *Adv. Healthcare Mater.*, 2023, **12**, 2300530.
23 T. Xiong, Y. Chen, M. Li, X. Chen and X. Peng, *Small*, 2025, **21**, 2501911.
24 E. J. Anthony, E. M. Bolitho, H. E. Bridgewater, O. W. L. Carter, J. M. Donnelly, C. Imberti, E. C. Lant, F. Lermyte, R. J. Needham, M. Palau, P. J. Sadler, H. Shi, F.-X. Wang, W.-Y. Zhang and Z. Zhang, *Chem. Sci.*, 2020, **11**, 12888–12917.
25 Y. Zhang, B.-T. Doan and G. Gasser, *Chem. Rev.*, 2023, **123**, 10135–10155.
26 S. A. McFarland, A. Mandel, R. Dumoulin-White and G. Gasser, *Curr. Opin. Chem. Biol.*, 2020, **56**, 23–27.
27 A. Zamora, G. Vigueras, V. Rodríguez, M. D. Santana and J. Ruiz, *Coord. Chem. Rev.*, 2018, **360**, 34–76.
28 J. Sanz-Villafruela, A. Carbayo, M. Martínez-Alonso and G. Espino, *Coord. Chem. Rev.*, 2025, **534**, 216572.
29 L. C.-C. Lee and K. K.-W. Lo, *J. Am. Chem. Soc.*, 2022, **144**, 14420–14440.
30 V. Novohradsky, G. Vigueras, J. Pracharova, N. Cutillas, C. Janiak, H. Kostrhunova, V. Brabec, J. Ruiz and J. Kasparkova, *Inorg. Chem. Front.*, 2019, **6**, 2500–2513.
31 J. Kasparkova, A. Hernández-García, H. Kostrhunova, M. Goicuría, V. Novohradsky, D. Bautista, L. Markova, M. D. Santana, V. Brabec and J. Ruiz, *J. Med. Chem.*, 2024, **67**, 691–708.
32 M. Park, J. S. Nam, T. Kim, G. Yoon, S. Kim, C. Lee, C. G. Lee, S. Park, K. S. Bejoymohandas, J. Yang, Y. H. Kwon, Y. J. Lee, J. K. Seo, D. Min, T. Park and T.-H. Kwon, *Adv. Sci.*, 2025, **12**, 2407236.
33 Q. Zhang, D. Chen, X. Liu, Z. Deng, J. Li, S. Zhu, B. Ma, R. Liu and H. Zhu, *Small*, 2025, **21**, 2403165.
34 A. Linero-Artiaga, L.-M. Servos, V. Rodríguez, J. Ruiz and J. Karges, *J. Med. Chem.*, 2025, **68**, 7792–7806.
35 A. Linero-Artiaga, L.-M. Servos, Z. Papadopoulos, V. Rodríguez, J. Ruiz and J. Karges, *Inorg. Chem. Front.*, 2025, DOI: [10.1039/D5QI01287B](10.1039/D5QI01287B).
36 S. Li, H. Yuan, X.-Z. Yang, X. Xu, W. Yu, Y. Wu, S. Yao, J. Xie, W. He, Z. Guo and Y. Chen, *ACS Cent. Sci.*, 2025, **11**, 441–451.
37 G. Vigueras, G. Gasser and J. Ruiz, *Dalton Trans.*, 2025, **54**, 1320–1328.
38 V. Novohradsky, A. Rovira, C. Hally, A. Galindo, G. Vigueras, A. Gandioso, M. Svitelova, R. Bresolí-Obach, H. Kostrhunova, L. Markova, J. Kasparkova, S. Nonell, J. Ruiz, V. Brabec and V. Marchán, *Angew. Chem., Int. Ed.*, 2019, **58**, 6311–6315.
39 V. Novohradsky, L. Markova, H. Kostrhunova, J. Kasparkova, J. Ruiz, V. Marchán and V. Brabec, *Chem. – Eur. J.*, 2021, **27**, 8547–8556.
40 A. Rovira, E. Ortega-Forte, C. Hally, M. Jordà-Redondo, D. Abad-Montero, G. Vigueras, J. I. Martínez, M. Bosch, S. Nonell, J. Ruiz and V. Marchán, *J. Med. Chem.*, 2023, **66**, 7849–7867.
41 E. Ortega-Forte, A. Rovira, P. Ashoo, E. Izquierdo-García, C. Hally, D. Abad-Montero, M. Jordà-Redondo, G. Vigueras, A. Deyà, J. L. Hernández, J. Galino, M. Bosch, M. E. Alberto, A. Francés-Monerris, S. Nonell, J. Ruiz and V. Marchán, *Inorg. Chem. Front.*, 2025, **12**, 3367–3383.
42 C. Huang, C. Liang, T. Sadhukhan, S. Banerjee, Z. Fan, T. Li, Z. Zhu, P. Zhang, K. Raghavachari and H. Huang, *Angew. Chem., Int. Ed.*, 2021, **60**, 9474–9479.
43 Z. Fan, J. Xie, T. Sadhukhan, C. Liang, C. Huang, W. Li, T. Li, P. Zhang, S. Banerjee, K. Raghavachari and H. Huang, *Chem. – Eur. J.*, 2022, **28**, e202103346.
44 A. K. Yadav, A. Upadhyay, A. Bera, R. Kushwaha, A. A. Mandal, S. Acharjee, A. Kunwar and S. Banerjee, *Inorg. Chem. Front.*, 2024, **11**, 5435–5448.
45 Y. Sun, X. Yan, Q. Wu, F. Zhang, Y. Pei, H. Su, W. Huang, Z. He, D. Zhu, D. Yan, D. Wang and B. Z. Tang, *Adv. Funct. Mater.*, 2025, 2508014.
46 G. Vigueras, E. Izquierdo-García, E. de la Torre-Rubio, D. Abad-Montero, M. D. Santana, V. Marchán and J. Ruiz, *Inorg. Chem. Front.*, 2025, **12**, 4355–4375.
47 J. Bonelli, E. Ortega-Forte, G. Vigueras, J. Follana-Berná, P. Ashoo, D. Abad-Montero, N. Isidro, M. López-Corrales, A. Hernández, J. Ortiz, E. Izquierdo-García, M. Bosch, J. Rocas, Á. Sastre-Santos, J. Ruiz and V. Marchán, *ACS Appl. Mater. Interfaces*, 2024, **16**, 38916–38930.
48 L. Qiao, J. Liu, S. Kuang, X. Liao, J. Kou, L. Ji and H. Chao, *Dalton Trans.*, 2021, **50**, 14332–14341.
49 N. Xu, H. Fang, Z. Zhu, Y. Su and Z. Su, *J. Med. Chem.*, 2025, **68**, 21489–21501.
50 H. Huang, S. Banerjee, K. Qiu, P. Zhang, O. Blacque, T. Malcomson, M. J. Paterson, G. J. Clarkson, M. Staniforth, V. G. Stavros, G. Gasser, H. Chao and P. J. Sadler, *Nat. Chem.*, 2019, **11**, 1041–1048.

51 V. Novohradsky, A. Marco, M. Svitelova, N. Cutillas, J. Ruiz and V. Brabec, *ACS Pharmacol. Transl. Sci.*, 2025, **8**, 2033–2047.

52 Z. Fan, Y. Rong, T. Sadhukhan, S. Liang, W. Li, Z. Yuan, Z. Zhu, S. Guo, S. Ji, J. Wang, R. Kushwaha, S. Banerjee, K. Raghavachari and H. Huang, *Angew. Chem., Int. Ed.*, 2022, **61**, e202202098.

53 L. Wei, R. Kushwaha, A. Dao, Z. Fan, S. Banerjee and H. Huang, *Chem. Commun.*, 2023, **59**, 3083–3086.

54 Q. Lie, H. Jiang, X. Lu, Z. Chen, J. Liang, Y. Zhang and H. Chao, *J. Med. Chem.*, 2025, **68**, 8894–8906.

55 L. Tu, C. Li, Q. Ding, A. Sharma, M. Li, J. Li, J. S. Kim and Y. Sun, *J. Am. Chem. Soc.*, 2024, **146**, 8991–9003.

56 L. Holden, R. C. Curley, G. Avella, C. Long and T. E. Keyes, *Angew. Chem., Int. Ed.*, 2024, **63**, e202408581.

57 K. Arora, M. Herroon, M. H. Al-Afyouni, N. P. Toupin, T. N. Rohrabaugh, L. M. Loftus, I. Podgorski, C. Turro and J. J. Kodanko, *J. Am. Chem. Soc.*, 2018, **140**, 14367–14380.

58 S. Monro, K. L. Colón, H. Yin, J. Roque, P. Konda, S. Gujar, R. P. Thummel, L. Lilge, C. G. Cameron and S. A. McFarland, *Chem. Rev.*, 2019, **119**, 797–828.

59 J. Karges, F. Heinemann, M. Jakubaszek, F. Maschietto, C. Subecz, M. Dotou, R. Vinck, O. Blacque, M. Tharaud, B. Goud, E. Viñuelas Zahinos, B. Spingler, I. Ciofini and G. Gasser, *J. Am. Chem. Soc.*, 2020, **142**, 6578–6587.

60 M.-F. Wang, R. Yang, S.-J. Tang, Y.-A. Deng, G.-K. Li, D. Zhang, D. Chen, X. Ren and F. Gao, *Angew. Chem., Int. Ed.*, 2022, **61**, e202208721.

61 J. A. Roque III, H. D. Cole, P. C. Barrett, L. M. Lifshits, R. O. Hodges, S. Kim, G. Deep, A. Francés-Monerris, M. E. Alberto, C. G. Cameron and S. A. McFarland, *J. Am. Chem. Soc.*, 2022, **144**, 8317–8336.

62 T. Sainuddin, J. McCain, M. Pinto, H. Yin, J. Gibson, M. Hetu and S. A. McFarland, *Inorg. Chem.*, 2016, **55**, 83–95.

63 X.-C. Li, Y. Liu, M. S. Liu and A. K.-Y. Jen, *Chem. Mater.*, 1999, **11**, 1568–1575.

64 Z. Lv, H. Wei, Q. Li, X. Su, S. Liu, K. Y. Zhang, W. Lv, Q. Zhao, X. Li and W. Huang, *Chem. Sci.*, 2018, **9**, 502–512.

65 J. A. Solís-Ruiz, A. Barthe, G. Riegel, R. O. Saavedra-Díaz, C. Gaiddon and R. Le Lagadec, *J. Inorg. Biochem.*, 2020, **208**, 111080.

66 M. Martínez-Alonso, A. Gandioso, C. Thibaudeau, X. Qin, P. Arnoux, N. Demeubayeva, V. Guérineau, C. Frochot, A. C. Jung, C. Gaiddon and G. Gasser, *ChemBioChem*, 2023, **24**, e202300203.

67 J. McCain, K. L. Colón, P. C. Barrett, S. M. A. Monro, T. Sainuddin, J. Roque III, M. Pinto, H. Yin, C. G. Cameron and S. A. McFarland, *Inorg. Chem.*, 2019, **58**, 10778–10790.

68 G. Ghosh, K. L. Colón, A. Fuller, T. Sainuddin, E. Bradner, J. McCain, S. M. A. Monro, H. Yin, M. W. Hetu, C. G. Cameron and S. A. McFarland, *Inorg. Chem.*, 2018, **57**, 7694–7712.

69 F. J. Ballester, E. Ortega, D. Bautista, M. D. Santana and J. Ruiz, *Chem. Commun.*, 2020, **56**, 10301–10304.

70 J. Cervinka, A. Hernández-García, D. Bautista, L. Markova, H. Kostrhunova, J. Malina, J. Kasparkova, M. D. Santana, V. Brabec and J. Ruiz, *Inorg. Chem. Front.*, 2024, **11**, 3855–3876.

71 A. Marco, J. Kasparkova, D. Bautista, H. Kostrhunova, N. Cutillas, L. Markova, V. Novohradsky, J. Ruiz and V. Brabec, *J. Med. Chem.*, 2024, **67**, 21470–21485.

72 E. Ortega-Forte, A. Rovira, M. López-Corrales, A. Hernández-García, F. J. Ballester, E. Izquierdo-García, M. Jordà-Redondo, M. Bosch, S. Nonell, M. D. Santana, J. Ruiz, V. Marchán and G. Gasser, *Chem. Sci.*, 2023, **14**, 7170–7184.

73 D. Abad-Montero, A. Gandioso, E. Izquierdo-García, S. Chumillas, A. Rovira, M. Bosch, M. Jordà-Redondo, D. Castaño, J. Bonelli, V. V. Novikov, A. Deyà, J. L. Hernández, J. Galino, M. E. Alberto, A. Francés-Monerris, S. Nonell, G. Gasser and V. Marchán, *J. Am. Chem. Soc.*, 2025, **147**, 7360–7376.

74 Z. Zhang, X. Zeng, X. Zhou, Z. Ma, M. He, D. Zhou, S. Long, J. Fan, X. Peng and W. Sun, *Angew. Chem., Int. Ed.*, 2025, e202512296.

75 Y. Qin, M. Lu and X. Gong, *Cell Biol. Int.*, 2008, **32**, 224–228.

76 L. Burnaugh, K. Sabeur and B. A. Ball, *Theriogenology*, 2007, **67**, 580–589.

77 S. Iravani and G. J. Soofi, in *Electron Spin Resonance Spectroscopy in Medicine*, ed. A. K. Shukla, Springer Singapore, Singapore, 2019, pp. 73–81.

78 H. Zhao, J. Joseph, H. Zhang, H. Karoui and B. Kalyanaraman, *Free Radicals Biol. Med.*, 2001, **31**, 599–606.

79 A. K. Yadav, R. Kushwaha, A. A. Mandal, A. Mandal and S. Banerjee, *J. Am. Chem. Soc.*, 2025, **147**, 7161–7181.

80 L. Wei, A. Dao, G. Yuan, P. Zhang and H. Huang, *Acc. Chem. Res.*, 2025, **58**, 2640–2651.

81 G. Vigueras, L. Markova, V. Novohradsky, A. Marco, N. Cutillas, H. Kostrhunova, J. Kasparkova, J. Ruiz and V. Brabec, *Inorg. Chem. Front.*, 2021, **8**, 4696–4711.

82 R. Wu, J. Yuen, E. Cheung, Z. Huang and E. Chu, *Photodiagn. Photodyn. Ther.*, 2024, **45**, 103975.

83 A. A. Abdelrahim, S. Hong and J. M. Song, *Anal. Chem.*, 2022, **94**, 13936–13943.